

Ruthenium Complexes



Ruthenium Complexes of Tripodal Ligands with Pyridine and Triazole Arms: Subtle Tuning of Thermal, Electrochemical, and Photochemical Reactivity

Fritz Weisser,^[a] Stephan Hohloch,^[a] Sebastian Plebst,^[b] David Schweinfurth,^[a] and Biprajit Sarkar^{*[a]}

Abstract: Electrochemical and photochemical bond-activation steps are important for a variety of chemical transformations. We present here four new complexes, $[\text{Ru}(\text{L}^n)(\text{dmsO})(\text{Cl})]\text{PF}_6$ (**1–4**), where L^n is a tripodal amine ligand with 4– n pyridylmethyl arms and $n-1$ triazolylmethyl arms. Structural comparisons show that the triazoles bind closer to the Ru center than the pyridines. For L^2 , two isomers (with respect to the position of the triazole arm, equatorial or axial), *trans-2_{sym}* and *trans-2_{unr}*, could be separated and compared. The increase in the number of the triazole arms in the ligand has almost no effect on the $\text{Ru}^{\text{II}}/\text{Ru}^{\text{III}}$ oxidation potentials, but it increases the stability of the $\text{Ru}-\text{S}_{\text{dmsO}}$ bond.

Hence, the oxidation waves become more reversible from *trans-1* to *trans-4*, and whereas the dmsO ligand readily dissociates from *trans-1* upon heating or irradiation with UV light, the $\text{Ru}-\text{S}$ bond of *trans-4* remains perfectly stable under the same conditions. The strength of the $\text{Ru}-\text{S}$ bond is not only influenced by the number of triazole arms but also by their position, as evidenced by the difference in redox behavior and reactivity of the two isomers, *trans-2_{sym}* and *trans-2_{unr}*. A mechanistic picture for the electrochemical, thermal, and photochemical bond activation is discussed with data from NMR spectroscopy, cyclic voltammetry, and spectroelectrochemistry.

Introduction

The tetradentate tripodal ligand, TPA [tris(2-pyridylmethyl)amine], and its derivatives have been widely used in coordination chemistry during the last decades.^[1] Its σ -donating central amine, its three π -accepting pyridylmethyl arms, and the mobility of these arms allow TPA to accommodate a variety of metal centers with very different coordination geometries and electronic structures.^[1] These properties make it an ideal ligand for the synthesis of redox or catalytically active species, because TPA can adapt to electronic and steric changes at the metal center.

Therefore, TPA and its derivatives have often been used to synthesize model complexes of metalloenzymes^[1a,1,m] and to

generate high-valent metal-oxo species,^[1] which play an important role as active intermediates in various oxidases and oxygenases.^[1l,m] $\text{Ru}^{\text{IV}}=\text{O}$ complexes with TPA showed high reactivity towards the oxidative functionalization of alkanes.^[1h,9] This kind of functionalization is key to a more economical use of natural resources like oil, coal, and gas. Various Ru complexes of TPA catalyze the oxidation, epoxidation, and hydroxylation of alkanes and alkenes.^[1h–j,2]

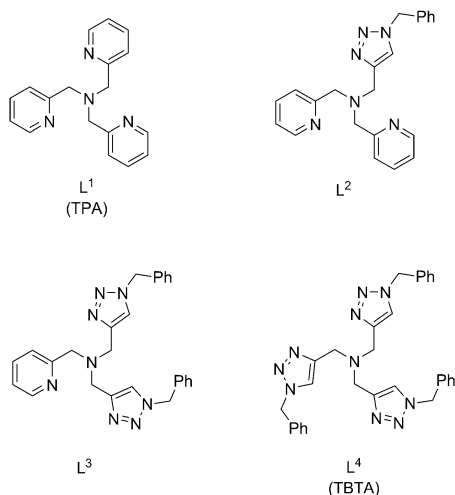
Yamaguchi et al. used complexes of the formula, $[(\text{L})\text{Ru}(\text{dmsO})(\text{Cl})]^+$, where L is TPA or one of its derivatives, to catalyze the conversion of adamantane into the corresponding alcohols.^[3] They investigated the effect of different substituents in position 5 of the pyridyl moieties of TPA on the reactivity of the complexes. They could show that the addition of methoxy-carbonyl groups increased the catalytic activity of the complexes. This kind of complex screening through ligand tuning is required for the development of effective catalytic systems. The most common efforts to tune the electronic and steric properties of TPA have included adding and varying substituents in positions 5 and 6 of the pyridyl arms.^[1]

An exceptionally efficient method for the easy variation of ligands and the modular build-up of compound libraries is the copper-catalyzed azide-alkyne cycloaddition, one of the click reactions.^[4] In recent years, this synthetic method has gained a lot of attention, and the resulting triazoles have found more and more applications as ligands in coordination chemistry.^[5] For example, triazole analogues of bipyridine (bpy) and terpyridine (terpy) have been used to synthesize complexes that

[a] F. Weisser, S. Hohloch, Dr. D. Schweinfurth, Prof. Dr. B. Sarkar
Institut für Chemie und Biochemie, Freie Universität Berlin
Fabeckstraße 34–36, 14195 Berlin (Germany)
Fax: (+49) 30-838-53310
E-mail: biprajit.sarkar@fu-berlin.de

[b] S. Plebst
Institut für Anorganische Chemie, Universität Stuttgart
Pfaffenwaldring 55, 70550 Stuttgart (Germany)

Supporting information for this article is available on the WWW under <http://dx.doi.org/10.1002/chem.201303640> and includes ^1H NMR spectra of the complexes in different solvents, cyclic voltammograms, differential pulse voltammograms, CV simulations, EPR spectra, UV/Vis spectra, spectroelectrochemistry, structure-refinement parameters, reactivity experiments monitored with ^1H NMR and UV/Vis spectroscopy, and kinetic studies of the light-driven DMSO exchange.



Scheme 1. Tripodal ligands L¹–L⁴.

show interesting differences to their bpy and terpy counterparts.^[5,6] Although this method has been used to create TPA analogues and derivatives,^[7] there has been no systematic investigation of the effect of the pyridine–triazole substitution on the properties of metal complexes.

In our work with triazole ligands, we have investigated the coordination chemistry of tris[(1-benzyl-1*H*-1,2,3-triazol-4-yl)methyl]amine (TBTA),^[8] a tripodal, tetradentate ligand, which looks very similar to TPA (Scheme 1). In TBTA, the pyridyl groups of TPA are replaced with *N*-benzyltriazolyl groups. By using click chemistry, the substituents at the triazole ring can be readily changed, thus allowing for the easy variation of steric demand, the introduction of additional donors, or the anchoring of complexes on surfaces. When we investigated 3d transition metal complexes of TBTA, we noticed significant, at times drastic, differences in their electronic and magnetic properties, as well as their reactivity, compared to their TPA counterparts.^[8]

The prospect of easily tunable ligand derivatives led us to apply this ligand system to the field of Ru–TPA complexes. By successively replacing the pyridyl arms of TPA with triazolyl groups, it should be possible to tune the electronic properties and the reactivity of the corresponding Ru complexes. In this work, we present a series of Ru^{II} complexes of the formula, [Ru(L^{*n*})(dmsO)(Cl)]PF₆ (1–4), where L^{*n*} (*n* = 1–4) is a tripodal, tetradentate ligand with *n*–1 triazole arms and 4–*n* pyridyl arms (Scheme 1 and 2). We investigated the electronic and spectroscopic properties of these com-

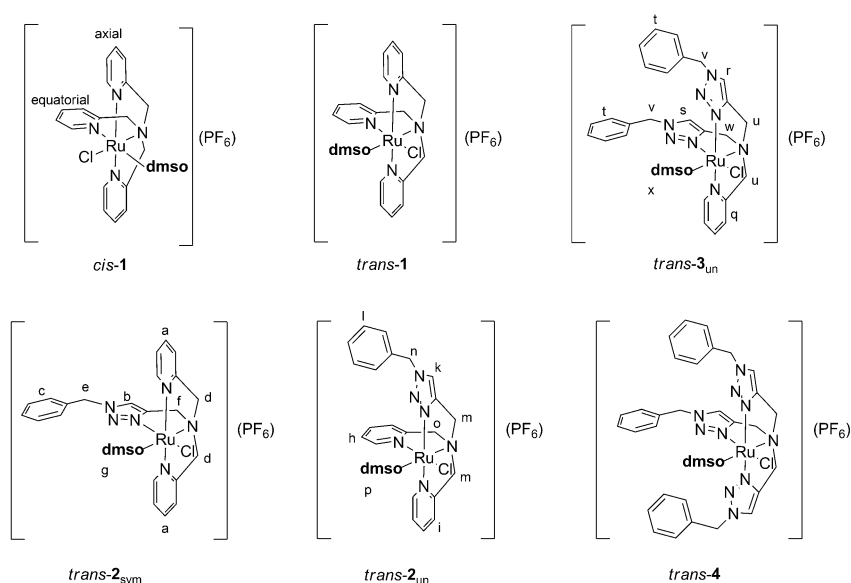
plexes to study the effect of the triazole–pyridine substitution on the reactivity and redox behavior of this system.

Results and Discussion

Synthesis and ¹H NMR spectroscopy

The ligands, TPA (L¹)^[9] and TBTA (L⁴),^[10] were synthesized by reported procedures. Even though the mixed-donor ligands L² and L³ (Scheme 1) were reported previously,^[7a] we have used an alternate synthetic route for their synthesis (see the Supporting Information). The click reaction for the synthesis of L² and L³ was carried out by using Cu^I–*N*-heterocyclic carbene complexes, as pioneered in our research group as catalysts.^[11] This method required low catalyst loadings and provided the ligands in good yields.

Previous work by Yamaguchi et al. showed that the complex [Ru(L)(dmsO)(Cl)]⁺ with L = TPA forms two isomers with respect to the position of the chlorido and the dmsO ligand.^[3] One isomer has the dmsO ligand *trans* to the central amine nitrogen atom of TPA (from here on referred to as “*trans* isomer”, Scheme 2) and the other isomer has the dmsO ligand positioned *cis* to the central nitrogen atom (“*cis* isomer”, Scheme 2). Under reaction conditions with short heating (heating at reflux in methanol for 2 h), both the *cis* and the *trans* isomer are formed, and they can be isolated by fractioned recrystallization in 47 and 29% yield, respectively. The two isomers can be clearly distinguished by the resonances of the dmsO ligand in the ¹H NMR spectrum. The dmsO methyl groups of the *cis* isomer show a singlet at 2.9 ppm in CDCl₃, whereas the corresponding singlet of the *trans* isomer appears at 3.5 ppm. Yamaguchi et al. could also show that the *cis* isomer is thermodynamically more stable than the *trans* isomer. When the *trans* isomer is heated in DMSO at 100 °C, it transforms into the *cis* isomer.



Scheme 2. Complexes [Ru(L^{*n*})(dmsO)(Cl)]PF₆. ¹H NMR resonances assigned to the indicated protons (a–x) are shown in Figure 1.

The conditions used for the complex synthesis in this work were slightly different, that is, the Ru precursor and the tripodal ligand were heated at reflux overnight (ca. 12 h). Under these conditions, the *trans*–*cis* ratios, determined from ¹H NMR spectra of the crude products, vary with the tripodal ligand. With L¹ (TPA, complex 1), the *cis* isomer was formed exclusively, whereas with L⁴ (TBTA, complex 4), the *trans* isomer was formed exclusively, and the complexes of L² and L³ (complexes 2 and 3) have *cis*–*trans* ratios of 1:4 and 1:15, respectively. In Table 1, the positions of the signals assigned to the dmsol methyl groups of the isomers are listed (see Figures S19 and S20 in the Supporting Information). For the complexes with L²–L⁴, only the *trans* isomers were isolated after column chromatography.

Table 1. ¹H NMR chemical shifts of the methyl groups of the dmsol ligands in crude products of 1–4 in CDCl₃. Percentage of the respective isomers (see Scheme 1) is given in parentheses.

	<i>Trans</i> / <i>un</i> [ppm], ([%])	<i>Trans</i> / <i>sym</i> [ppm], ([%])	<i>Cis</i> / <i>un</i> [ppm], ([%])	<i>Cis</i> / <i>sym</i> [ppm], ([%])
1		3.50 ^[a]		2.92 (100)
2	3.47, 3.59 (55)	3.68 (27)	2.89, 3.01 (11)	2.93 (7)
3	3.51, 3.84 (86)	3.56 (8)	2.92, 2.99 (3)	2.97 (3)
4		3.66 (100)		

[a] Obtained under different reaction conditions, see Ref. [13].

Complexes 2 and 3, with their mixed tripodal ligands, also form isomers with respect to the position of the individual arms. Together with the chlorido and the dmsol ligand, the tripodal ligand forms an octahedral coordination environment around the Ru center. This results in two distinct positions of the tripod arms. One arm is positioned in a plane with the chloride, the dmsol, and the central nitrogen atom of the tripod, and it is referred to in this work as the “equatorial arm”. The remaining two arms are positioned *trans* to each other, orthogonal to the abovementioned plane, and they are referred to as the “axial arms”. For 2, where L² has one triazole arm, this triazole can be in the equatorial or in an axial position. The isomer with the triazole in the equatorial position has a mirror plane through Cl–Ru–S–N_{amine} and is therefore referred to as the symmetrical isomer, *trans*-2_{sym} (compared to the unsymmetrical isomer *trans*-2_{un}, Scheme 2).

In the case of *trans*-2, the two isomers could be separated by column chromatography. The structure of each isomer could be determined by their ¹H NMR spectra in CD₃CN (Figure 1). *Trans*-2_{sym} has two identical pyridine arms and, therefore, exhibits only one set of pyridine signals (two doublets, two triplets; Figure 1, signals a) in the aromatic region. The CH₂ groups of the two identical 2-methylpyridyl arms have two hydrogen atoms with different chemical environments, thus resulting in geminal coupling, which can be observed in the form of two pseudo doublets with large coupling constants ($J_{AB} = 15$ Hz) in the range 4.70–5.80 ppm (Figure 1, signals d). The two CH₂ groups of the triazole arm each have two chemically identical protons, and, for each CH₂ group, a singlet

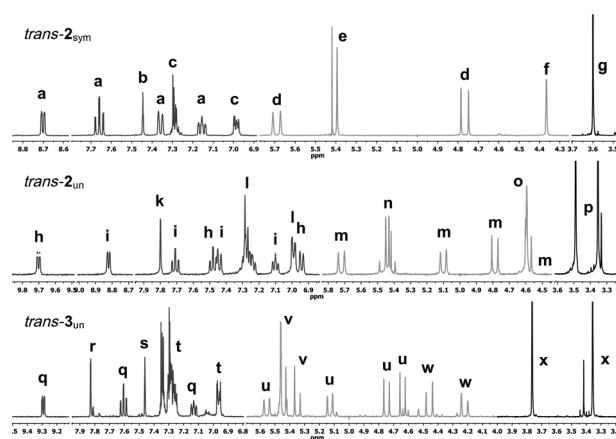


Figure 1. ¹H NMR spectra measured in CD₃CN. For assignment of the signals see Scheme 2.

(at 4.37 and 5.40 ppm) is observed (Figure 1, signals e and f). Finally, because of the symmetrical coordination environment, the dmsol methyl groups of *trans*-2_{sym} only show one singlet, which integrates for six protons (Figure 1, signal g).

The unsymmetrical isomer, *trans*-2_{un}, has two different pyridine arms, one in an axial and one in an equatorial position. Therefore, its ¹H NMR spectrum shows two sets of pyridine signals (four doublets, four triplets; Figure 1, signals h and i) in the aromatic region. All four CH₂ groups are different, and three of them have two protons with different chemical environments. This difference leads to geminal coupling and results in six pseudo doublets with large coupling constants ($J_{AB} = 14$ –15 Hz) and one singlet in the range 4.50–5.80 ppm (Figure 1, signals m–o). Finally, because of the unsymmetrical coordination environment, the dmsol methyl groups of *trans*-2_{un} show two singlets, which each integrate for three protons (Figure 1, signal p). For *trans*-3, the symmetrical and the unsymmetrical isomers could not be separated, and the resonances of the major isomer, *trans*-3_{un}, are assigned in Scheme 2. By comparing the integrals of the resonances of the dmsol methyl group, in the ¹H NMR spectra of crude 2 and 3, the ratios of the symmetrical to the unsymmetrical isomers could be determined. The ratio *trans*-2_{sym}/*trans*-2_{un} is approximately 1:2, and the ratio *trans*-3_{sym}/*trans*-3_{un} is approximately 1:10.

Crystal structures

Single crystals of *trans*-2_{sym} (Figure 2), *trans*-2_{un} (Figure 3), and *trans*-3_{un} (Figure 4) suitable for X-ray diffraction structure analyses could be obtained. The orientations of the ligands in the crystal structures match the structures of the complexes predicted from the ¹H NMR data. Table 2 shows a comparison of important distances and angles of the three new structures (*trans*-2_{sym}, *trans*-2_{un}, and *trans*-3_{un}) and two structures from the literature (*cis*-1,^[3] *trans*-1^[3]). In the order *trans*-1 < *trans*-2 < *trans*-3, that is, with an increasing number of triazole arms, the Ru–N_{amine} distance increases from 2.095(2) to 2.134(4) Å, whereas the distance Ru–S (*trans* to N_{amine}) slightly decreases in the same order, from 2.2653(8) to 2.2359(14) Å. The Ru–Cl distan-

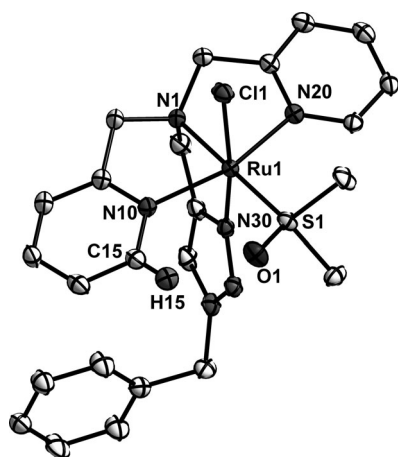


Figure 2. ORTEP view of *trans-2_{sym}*-acetone. Ellipsoids are drawn at the 50% probability level. H atoms, solvent molecules, and anions are omitted for clarity.

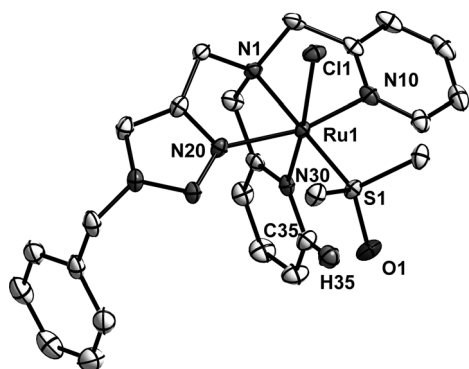


Figure 3. ORTEP view of *trans-2_{un}*. Ellipsoids are drawn at the 50% probability level. H atoms, solvent molecules, and anions are omitted for clarity.

ces of all five structures show no trend and vary only slightly around 2.43 Å.

In the order *trans-1* > *trans-2_{sym}* > *trans-2_{un}* > *trans-3_{un}* the sum of the Ru–N distances of the tripodal ligand decreases from 6.265(6) to 6.170(12) Å. With an increasing number of triazole arms, the arms of the tripodal ligand come closer to the metal center. A remarkable difference in bond lengths is observed for the two isomers *trans-2_{sym}* and *trans-2_{un}*. In the crystal structure of *trans-2_{sym}*, the triazole in the equatorial position exhibits a Ru–N distance of 2.031(3) Å, which is the shortest Ru–N distance observed in all five structures. The two pyridine rings of *trans-2_{sym}* are in the axial

positions *trans* to each other and have Ru–N bond lengths of 2.100(2) and 2.101(2) Å, which are among the longest Ru–N distances in all five structures. In contrast, in the crystal structure of unsymmetrical *trans-2_{un}*, the three arms show similar Ru–N distances in the range 2.066–2.076 Å. The Ru–N distances of the axial triazole and pyridine arm are 2.069(3) and 2.076(3) Å, respectively. Therefore, the comparison of the two *trans-2* isomers points to a push–pull effect between the mutually *trans* disposed σ -donating triazole ring and the π -accepting pyridine ring in *trans-2_{un}* (Table 2).

All five crystal structures show the Ru center in a distorted octahedral coordination environment, in which the axis N_{ax} –Ru– N_{ax} is the most distorted, angles being in the range 160.15(10)–163.45(10)°. For the compounds *trans-1*, *trans-2_{sym}*, *trans-2_{un}* and *trans-3_{un}*, the axis N_{amine} –Ru–S is the least distorted, with angles close to 180°, specifically, 176.13(7)–179.52(8)°. For these four compounds, the two axial rings (triazole or pyridine) are not coplanar, but they are bent away from the chlorido ligand. In *trans-2_{sym}* and *trans-3_{un}*, the triazole rings in the equatorial position are tilted out of the Ru–Cl–S– N_{amine} plane by 18.6(1) and 19.0(1)°, respectively. In *trans-1* and *trans-2_{un}*, there are pyridine rings in the equatorial position, and they are almost coplanar with Ru–Cl–S– N_{amine} , and the tilt angles are 1.8(5) and 2.8(1)°, respectively. It could be argued, whether the tilt of the equatorial ring is due to packing forces or the nature of the ring. However, for *cis-1*, there are three different structures reported,^[3,12] two of which have strongly tilted pyridine rings in the equatorial position.

Finally, the C and O atoms of the dmsoligand in *trans-1*, *trans-2_{sym}*, *trans-2_{un}* and *trans-3_{un}* are positioned in an eclipsed fashion with respect to the CH₂ groups of the tripodal ligand. In the structures with mixed tripodal ligands, the O_{dmsol} atom always points to a pyridyl ring, and there are short C_{py}–H_{py}...O_{dmsol} contacts with the H atom in the 6-position of that pyridyl ring.

Table 2. Comparison of important bond lengths [Å] and angles [°].

	<i>cis-1</i> ^[a]	<i>trans-1</i> ^[a]	<i>trans-2_{sym}</i> -acetone	<i>trans-2_{un}</i>	<i>trans-3_{un}</i>
Ru– N_{amine} [Å]	2.070(3)	2.095(2)	2.119(3)	2.112(3)	2.134(4)
Ru– N_{ax} [Å]	2.060(3)	2.091(2)	2.101(2)	2.069(3) ^[b]	2.057(4)
Ru– N_{eq} [Å]	2.078(3)	2.079(2)	2.100(2)	2.076(3)	2.061(4) ^[b]
Σ Ru– N_{arms} [Å]	2.106(3)	2.095(2)	2.031(3) ^[b]	2.066(3)	2.052(4) ^[b]
Σ Ru– N_{arms} [Å]	6.244(9)	6.265(6)	6.232(7)	6.211(9)	6.170(12)
Ru–S [Å]	2.2385(10)	2.2653(8)	2.2432(9)	2.2470(10)	2.2359(14)
Ru–Cl [Å]	2.4321(9)	2.4319(9)	2.4285(12)	2.4462(9)	2.4347(13)
S–O [Å]		1.479(3)	1.492(2)	1.484(3)	1.485(4)
S=O...H–C _{pyr} [Å]			2.28	2.22	2.57
N_{amine} –Ru– N_{ax} [°]	82.90(11)		78.14(9)	80.27(11)	82.02(16)
	80.55(10)		82.01(10)	80.52(11)	78.81(16)
N_{ax} –Ru– N_{ax} [°]	163.45(10)		160.15(10)	160.55(11)	160.77(17)
N_{amine} –Ru–S [°]	98.48(8)	176.13(7)	179.52(8)	176.89(8)	177.07(12)
N_{eq} –Ru–Cl [°]	92.62(7)		172.40(7)	172.43(8)	170.08(12)
S–Ru–Cl [°]	88.87(3)	85.75(3)	87.36(4)	87.10(3)	85.96(5)
\angle ring _{ax} –ring _{ax} [°]			24.02(8)	25.7(1)	26.2(2)
\angle ring _{eq} –(Ru–Cl– N_{amine} –S) [°]		1.80(5)	18.63(8) ^[b]	2.81(9)	19.0(1) ^[b]

[a] Ref. [3b]. [b] Bond or angle involves a triazole ring.

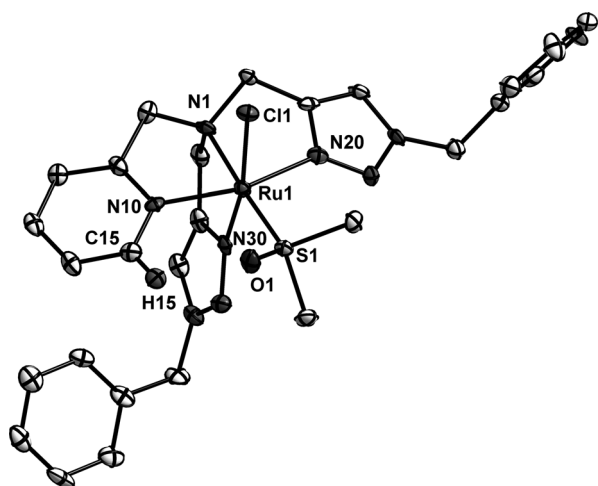


Figure 4. ORTEP view of *trans-3_{un}*. Ellipsoids are drawn at the 50% probability level. H atoms, solvent molecules, and anions are omitted for clarity.

Electrochemistry

Cyclic voltammetry of all six complexes was measured in CH_2Cl_2 and acetonitrile. All complexes show a quasireversible or reversible one-electron oxidation from Ru^{II} to Ru^{III} . The oxidation potentials versus the ferrocene–ferrocenium couple are listed in Table 3. In CH_2Cl_2 , the potentials vary in the range 0.58–0.71 V, and there is a trend towards slightly more cathodic potentials with an increasing number of triazole arms in the tripodal ligand (0.71 V for *trans-1*; 0.58 and 0.60 V for *trans-3* and *trans-4*, respectively). In acetonitrile, the variation of the oxidation potential is even smaller (0.58–0.62 V).

Although the oxidation waves in CH_2Cl_2 look reversible at scan rates of 100 mV s^{-1} or higher, the complexes *trans-1* and *trans-2_{sym}* show additional re-reduction peaks with cathodic peak potentials, E_{pcr} , of -0.06 and 0.05 V, respectively (Figure 5 and, in the Supporting Information, Figure S21). In the second cycle, there are new oxidation waves corresponding to these additional re-reduction processes (Figure 5). Because the whole effect is observed both in CH_2Cl_2 and acetonitrile, the effect is not due to coordinating solvent molecules. It is more pronounced at low scan rates, at which the intensity of the first re-reduction wave is very much diminished for *trans-1* and

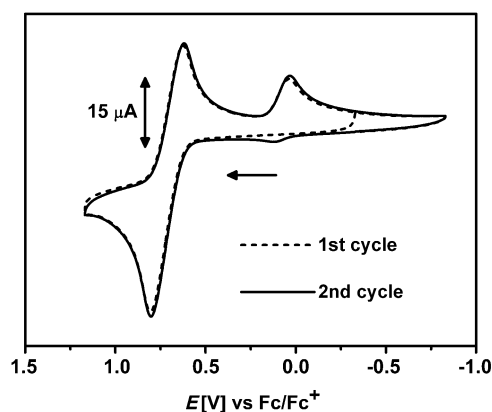


Figure 5. Cyclic voltammogram of *trans-1* in CH_2Cl_2 at 100 mV s^{-1} with 0.1 M Bu_4NPF_6 .

trans-2_{sym}. In the literature, the appearance of additional re-reduction peaks with similar anodic shifts (ca. 0.5 V) has been reported for other Ru–dmsO complexes. In these cases, the new re-reduction peaks were attributed to isomers with O-bound dmsO ligands instead of S-bound ones. The formation of such isomers through an EC mechanism upon oxidation of the Ru center has been observed before.^[13] Kojima et al. proposed that a key factor for the stability of the Ru–S bond is π back donation from a $d\pi$ Ru orbital to the S=O moiety of dmsO. According to this explanation, the decreased electron density at the Ru^{III} center upon oxidation would lead to a labilization of the Ru–S bond and hence result in a dissociation or coordinative rearrangement of the dmsO ligand.^[14]

We simulated the CVs of *trans-1* in acetonitrile with an EC mechanism at different scan rates by using the program DigElch7. The scan-rate-dependent behavior of the compound could be best reproduced by assuming a dissociation–association mechanism, in which the S-bound dmsO ligand of *trans-1*⁺ (one-electron-oxidized *trans-1*) dissociates and then re-coordinates through the oxygen atom. Working with a mechanism, in which dmsO dissociates and an excess component (acetonitrile solvent molecules) coordinates instead, the simulations could not reproduce the scan-rate-dependent behavior of *trans-1*. This seems to contrast with the findings of NMR studies of temperature-driven and UV-light-driven reactions of complexes 1–4 (see below), in which the dissociated dmsO ligand was replaced by a solvent molecule.

However, the re-coordination of dmsO can be rationalized by the fact that the current in the cyclic voltammograms is due to species and processes at the electrode surface, where there is a highly increased concentration of complex molecules, a condition that in return would result in an elevated concentration of dissociated dmsO molecules. Further away from the electrode, a replacement of dmsO by acetonitrile might occur, but this would not be reflected in the CV current. The simulations afforded an equilibrium constant of $K_{\text{eq}}=8$ for the combined dissociation–recoordination process of dmsO, data that is in good agreement with results obtained for a Ru^{II} –dmsO polypyridyl complex by Benet-Buchholz et al.^[13] Figure 6 shows a comparison of the simulated and the experimental CV of

Table 3. Oxidation potentials ($E_{1/2}$) and reduction peak potentials (E_p) measured in CH_2Cl_2 and acetonitrile at 100 mV s^{-1} with 0.1 M Bu_4NPF_6 at room temperature.

	$E_{1/2}(\text{Ox})$ in CH_2Cl_2 ^[a] [V]	$E_{1/2}(\text{Ox})$ in MeCN ^[a] [V]	$I_{\text{pc}}/I_{\text{pa}}$ in MeCN ^[b]	$E_p(\text{Red})$ in MeCN ^[a] [V]
<i>cis-1</i>	0.65	0.58	0.92	−2.41
<i>trans-1</i>	0.71	0.62	0.45	−2.31
<i>trans-2_{sym}</i>	0.65	0.61	0.63	−2.36
<i>trans-2_{un}</i>	0.68	0.62	0.77	−2.35
<i>trans-3_{un}</i>	0.62	0.60	0.99	−2.40
<i>trans-4</i>	0.60	0.59	0.99	−2.57

[a] vs. Fc/Fc^+ . [b] For the oxidation at 10 mV s^{-1} .

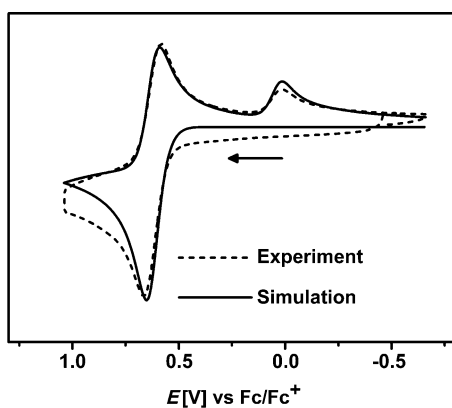


Figure 6. Comparison of a CV of *trans*-1 measured in acetonitrile at 250 mV s⁻¹ and a simulation.

trans-1 in acetonitrile at 250 mV s⁻¹. Details of the simulation parameters and voltammograms simulated at other scan rates are presented in the Supporting Information (Figure S26).

The cyclic voltammograms of all six complexes, measured in acetonitrile at 10 mV s⁻¹, were used to determine the corresponding peak-current ratios, I_{pc}/I_{pa} , which can be taken as a measure for the reversibility of the oxidation process (Figure 7 and, in the Supporting Information, Figure S22). The ratio is 1 for ideal systems and close to 0 for highly irreversible systems. The values of this ratio are also listed in Table 3, and

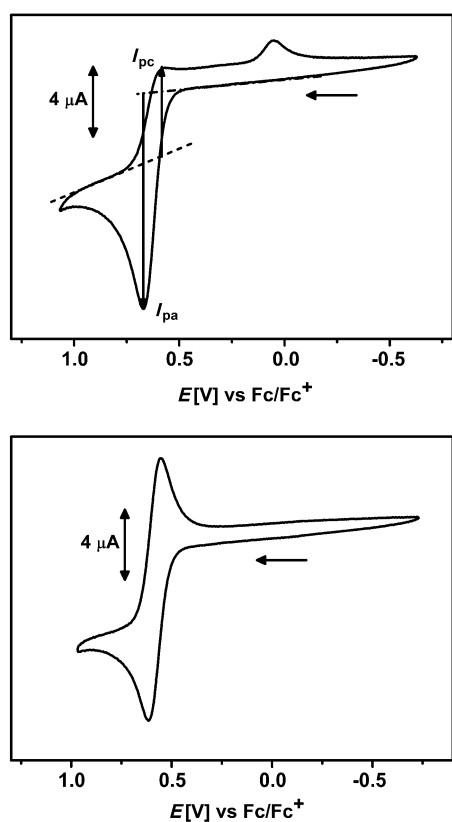


Figure 7. Cyclic voltammograms of *trans*-1 (top) and *trans*-4 (bottom) measured in acetonitrile at 10 mV s⁻¹ with 0.1 M Bu₄NPF₆ at room temperature.

they show that the oxidized species of *trans*-1, *trans*-1⁺, is much less stable than the isomer *cis*-1⁺. The stability of the one-electron-oxidized species, and hence the reversibility of the oxidation process, increases with the number of triazole arms at the tripodal ligand ($I_{pc}/I_{pa}=0.99$ for *trans*-3 and *trans*-4). Remarkably, the oxidation of *trans*-2_{un} is more reversible than that of *trans*-2_{sym}, which means that the position of the triazole arm has an effect on the redox stability of the complex. According to the abovementioned explanation of the observed EC phenomenon, the increased redox reversibility of the triazole-rich compounds points to a higher stability of the Ru–S bond in the oxidized state. This points to a higher electron density at the Ru center for complexes with more triazole arms. Hence, the substitution of triazolyl for pyridyl moieties has little effect on the oxidation potential but great effect on the redox stability of the complex.

In acetonitrile, all six complexes show an irreversible reduction close to the edge of the solvent window (see the Supporting Information, Figure S24). DPV measurements show that this reduction involves the same number of electrons as the oxidation (see the Supporting Information, Figure S25). Therefore, we attribute these redox waves to a one-electron reduction at the tripodal ligand. In agreement with this assignment, the reduction potentials shift to more negative values with an increasing number of triazole arms, a behavior that is due to the stronger donating and weaker accepting nature of the triazoles compared to the pyridines. As a result of this shift, the potential gap between oxidation and reduction, which to a first approximation often correlates to the HOMO–LUMO gap of a complex, increases from *trans*-1 to *trans*-4.

EPR and UV/Vis spectroelectrochemistry (SEC)

The measurement of EPR spectra of the oxidized species of 1–4 was hampered by the redox dynamic behavior discussed above. Only the two most stable complexes, *trans*-3_{un} and *trans*-4, showed good EPR spectra after electrolysis in CH₂Cl₂ at room temperature. For example, Figure 8 shows the EPR spectrum of oxidized *trans*-3_{un}. Apart from an isotropic signal at a *g* value close to that of the free electron, a signal that is probably due to residual dmsO impurities in the sample, the spec-

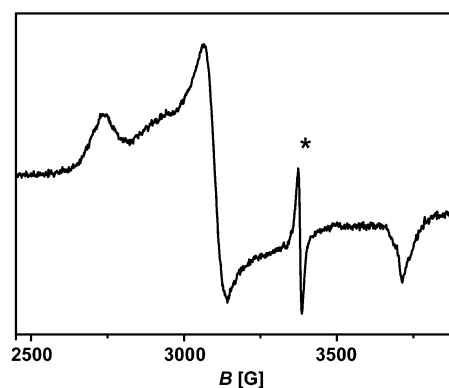


Figure 8. EPR spectrum of one-electron-oxidized *trans*-3_{un} recorded in CH₂Cl₂ at 110 K. The asterisk indicates the signal of an organic impurity.

Table 4. g values of the one-electron-oxidized complexes 1–4 measured in CH_2Cl_2 at 110 K with 0.1 M Bu_4NPF_6 .					
	g_1	g_2	g_3	Δg	g^*
<i>cis</i> -1	2.517	2.269	1.800	0.717	2.068
<i>trans</i> -1	–	–	–	–	2.062
<i>trans</i> -2 _{sym}	2.462	2.203	1.814	0.648	2.064
<i>trans</i> -2 _{un}	2.489	2.182	1.813	0.676	2.060
<i>trans</i> -3 _{un}	2.472	2.182	1.821	0.651	–
<i>trans</i> -4	2.454	2.178	1.821	0.633	–

trum shows an anisotropic signal with three g values, $g_1 = 2.472$, $g_2 = 2.182$, and $g_3 = 1.821$. This spectrum is typical for a metal-centered spin. For the complexes *cis*-1, *trans*-1, *trans*-2_{sym} and *trans*-2_{un}, EPR spectra could only be measured when the electrolysis was carried out at -40°C , so as to slow down the chemical reaction following the oxidation. In this way, *cis*-1, *trans*-2_{sym} and *trans*-2_{un} showed anisotropic spectra with g values similar to those of *trans*-3_{un} and *trans*-4 (Table 4). The less redox stable complexes show an additional signal with a g value (g^*) in the range 2.06–2.07, a signal that we tentatively attribute to the product of the dmsO rearrangement upon oxidation. The least oxidation stable complex, *trans*-1, exclusively shows an EPR signal with $g^* = 2.062$ (see the Supporting Information, Figures S27 and S28).

The UV/Vis spectra of 1–4 were recorded in CH_2Cl_2 (Figure 9) and acetonitrile (see the Supporting Information, Figure S31), showing identical bands in both solvents (see the Supporting Information, Table S1). The main features of the spectra are a band around 250 nm and bands between 300 and 450 nm. The band around 250 nm can be assigned to π – π^* transitions

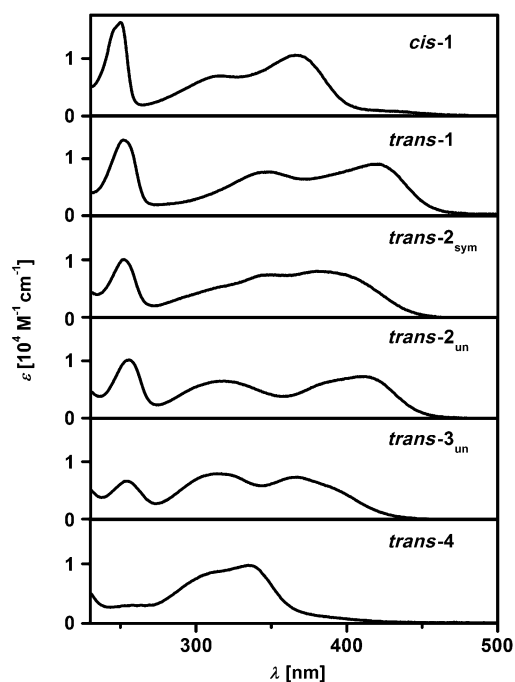


Figure 9. UV/Vis absorption spectra of the complexes 1–4 measured in CH_2Cl_2 .

of the pyridyl moieties. The intensity of this band decreases with the number of pyridine arms, and it completely disappears for *trans*-4.

On the basis of assignments for similar complexes,^[3,14] the absorption bands between 300 and 450 nm can be attributed to metal-to-ligand charge transfer (MLCT) from Ru $d\pi$ orbitals to $p\pi^*$ orbitals of the pyridine and triazole arms. From *trans*-1 to *trans*-4, the MLCT bands shift to shorter wavelengths, thus correlating to the increasing potential gap between oxidation and reduction in the CV (see above). In agreement with their assignment to MLCT transitions, the absorption bands between 300 and 450 nm decrease in intensity or disappear upon oxidation (for example, see Figure 10). The oxidation-stable complexes, *cis*-1, *trans*-3_{un} and *trans*-4, show isosbestic points in the SEC plots (see the Supporting Information, Figure S29). The complexes with more labile dmsO ligands (*trans*-1, *trans*-2_{sym}, *trans*-2_{un}) only initially show isosbestic points that are blurred in the course of the electrolysis by additional spectroscopic shifts owing to the dmsO rearrangement (see the Supporting Information, Figure S29). The observation that the redox stability of the complexes increases with the number of triazole arms is further corroborated by the UV/Vis spectra recorded before and after the SEC cycle for every complex (see the Supporting Information, Figure S30). With more triazole arms, the overlap of the two spectra becomes almost ideal, which points to a reversible oxidation process.

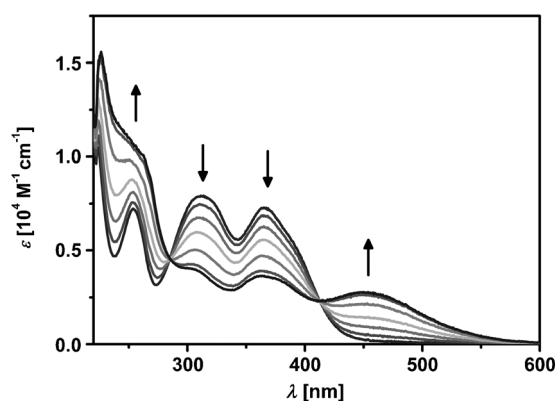


Figure 10. Change in the UV/Vis absorption of *trans*-3_{un} in the course of a one-electron oxidation in CH_2Cl_2 .

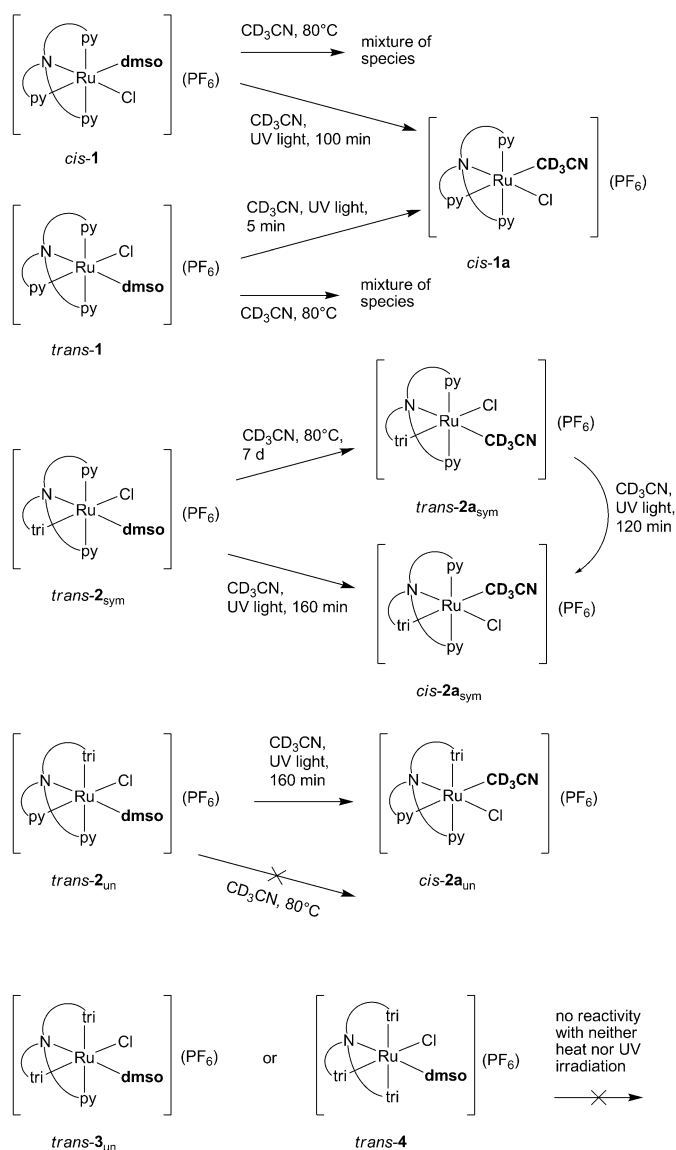
Thermo- and photoreactivity of 1–4

Prompted by the results of the CV measurements and previous reports about the thermo- and photo-induced reactivity of *cis*-1, *trans*-1, and related complexes,^[2b,3,15] we investigated the reactivity of all six complexes under heating or irradiation with UV light. The experiments were carried out in CD_3CN and $[\text{D}_6]\text{DMSO}$ and monitored by ^1H NMR spectroscopy. When complexes *cis*-1 and *trans*-1 are heated in CD_3CN at 80°C for seven days, they both form identical mixtures of several new species, and the resonance of free DMSO appears at 2.47 ppm (see the Supporting Information, Figure S33). Yamaguchi et al. were able to show that *trans*-1 converts to *cis*-1 upon heating in

[D₆]DMSO.^[3] When *cis*-1 and *trans*-1 are irradiated at 365 nm (a wavelength in the range of their MLCT bands) in CD₃CN, the NMR spectra of both show a clean conversion to product **1a**, and the signal at 2.47 ppm points to a loss of the DMSO ligand (see the Supporting Information, Figure S34). In another work, Yamaguchi et al. were able to show by mass spectrometry that, in **1a**, DMSO is substituted by acetonitrile. Hence, the MLCT transition leads to a decrease in the electron density at the metal center, a decrease that in turn weakens the Ru–S back bonding and leads to the dissociation and substitution of the dmsoligand.

For *trans*-1, the conversion to **1a** takes only 5 min, whereas for *cis*-1, which has a much more stable Ru–S_{dmsoligand} bond (see CV), irradiation for 100 min is needed to achieve a conversion of greater than 90% (see the Supporting Information, Figure S34). For *cis*-1, the corresponding irradiation experiment in [D₆]DMSO leads to the disappearance of the ¹H NMR signal of the dmsoligand (2.8 ppm) and the appearance of the free-DMSO resonance at 2.5 ppm (see the Supporting Information, Figures S35 and S48). All other resonances remain almost unchanged; only after prolonged irradiation, signals of *trans*-1 appear. For *trans*-1, irradiation in [D₆]DMSO leads to an ¹H NMR spectrum identical to that of *cis*-1, except for the signal of free DMSO and some remaining weak signals of *trans*-1 (see the Supporting Information, Figures S35 and S48). A closer look at the spectra shows that the prolonged irradiation of either *cis*-1 or *trans*-1 results in a *cis*-1/*trans*-1 ratio of approximately 95:5. Therefore, in the case of *cis*-1, irradiation primarily leads to a simple substitution of the dmsoligand by [D₆]dmsoligand, whereas in the case of *trans*-1, irradiation overwhelmingly leads to a substitution and to the isomerization to *cis*-1. Therefore, we assume that, analogously, the acetonitrile ligand in **1a** is in a position *cis* to the amine nitrogen atom (that is, *cis*-1a; see Scheme 3).

We analyzed the kinetics of the light-driven DMSO exchange in [D₆]DMSO more thoroughly. The complexes *cis*-1, *trans*-1, *trans*-2_{sym}, and *trans*-2_{un} were dissolved in [D₆]DMSO (3 mmol L⁻¹) and irradiated at 365 nm. ¹H NMR spectra were recorded after 10, 70, 190, 340, 520, and 760 min, and the concentrations of the original species with non-deuterated dmsoligands were determined (see the Supporting Information, Figures S44–S47 and S49, Table S3). The DMSO exchange of all four complexes follows pseudo-first-order kinetics (Figure 11 and, in the Supporting Information, Figures S49–S54), and the rate constants, *k*, for *cis*-1, *trans*-1, *trans*-2_{sym}, and *trans*-2_{un} are 1.36 × 10⁻⁴, 2.07 × 10⁻⁴, 0.35 × 10⁻⁴, and 0.62 × 10⁻⁴ s⁻¹, respectively (see the Supporting Information, Table S3). These data show that *trans*-1 is more reactive toward light-driven DMSO exchange than *cis*-1, behavior that is in agreement with CV measurements and thermal reactivity experiments (see above). Furthermore, the two isomers of *trans*-2, which have one triazole arm, are less reactive, that is, have more tightly bound dmsoligands, than complex *trans*-1, behavior that also agrees with CV and thermal-reactivity results. However, the fact that *trans*-2_{un} is more reactive in the light-driven DMSO exchange than the isomer *trans*-2_{sym} is in contrast to the CV results (see above) and to the thermal reactivity in CD₃CN (see below).



Scheme 3. Reaction Scheme proposed to explain the changes in the ¹H NMR spectra of **1–4** in CD₃CN observed upon heating and irradiation with UV light.

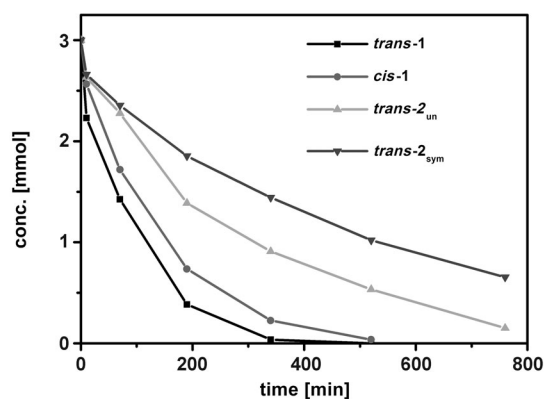


Figure 11. Concentrations of complexes with non-deuterated dmsoligands after different periods of irradiation at 365 nm in [D₆]-DMSO.

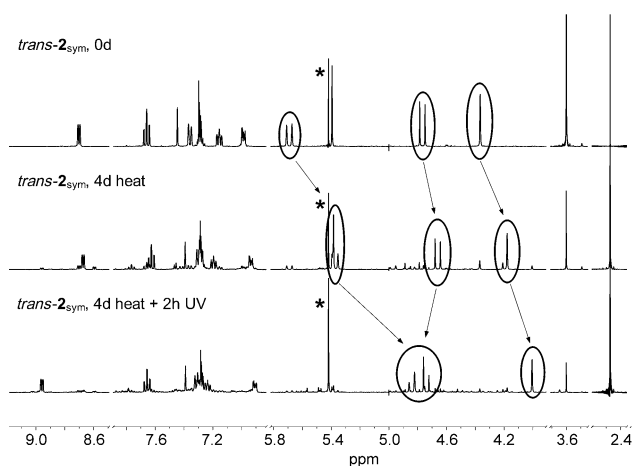


Figure 12. Changes in the ^1H NMR spectrum of $\text{trans-2}_{\text{sym}}$ in CD_3CN upon heating and subsequent irradiation with UV light.

For $\text{trans-2}_{\text{sym}}$, heating in CD_3CN at 80°C for four days leads to the formation of one major new species. The corresponding ^1H NMR spectrum (Figure 12 and, in the Supporting Information, Figure S36) shows the signal of free DMSO at 2.47 ppm and only one set of pyridine signals (two doublets, two triplets) in the aromatic region. Therefore, the new species must also be symmetrical with two identical pyridine arms and, presumably, an acetonitrile ligand. The unsymmetrical isomer, $\text{trans-2}_{\text{un}}$, which showed a slightly stronger binding of the dmsO ligand than $\text{trans-2}_{\text{sym}}$ in the CV, does not react under the same heating conditions (Scheme 3). Remarkably, the position of the triazole arm in trans-2 has a pronounced effect on the thermal stability of the complex.

When $\text{trans-2}_{\text{sym}}$ and $\text{trans-2}_{\text{un}}$ are irradiated at 365 nm in CD_3CN for 160 min, both complexes lose their dmsO ligand (signal of free DMSO in the ^1H NMR spectrum) and each form one major new species (see the Supporting Information, Figures S39 and S40). Mass spectra show that for both isomers of trans-2 , the dmsO ligand is substituted by a CD_3CN molecule (see the Supporting Information, Figures S42 and S43). In both cases, the major species has the same orientation of the tripod arms as the dmsO precursor: the species formed from $\text{trans-2}_{\text{sym}}$ upon irradiation shows one set of pyridine signals in the ^1H NMR spectrum and is, therefore, also symmetrical; the species formed from $\text{trans-2}_{\text{un}}$ shows two sets of pyridine signals and is, therefore, also unsymmetrical (Figure 13). The product formed from $\text{trans-2}_{\text{sym}}$ upon irradiation is different from the product formed upon heating (Figure 12 and, in the Supporting Information, Figures S36 and S39). When the heating product is further irradiated for 2 h, it converts to the irradiation product (Figure 12), but heating the irradiation product has no effect.

To further investigate the difference between the heating and irradiation product of $\text{trans-2}_{\text{sym}}$, the experiments were repeated in $[\text{D}_6]\text{DMSO}$. When a $[\text{D}_6]\text{DMSO}$ solution of $\text{trans-2}_{\text{sym}}$ was heated at 80°C for seven days, the ^1H NMR signal of the coordinated DMSO completely disappeared, but the other signals of the complex only lost a third of their original intensity

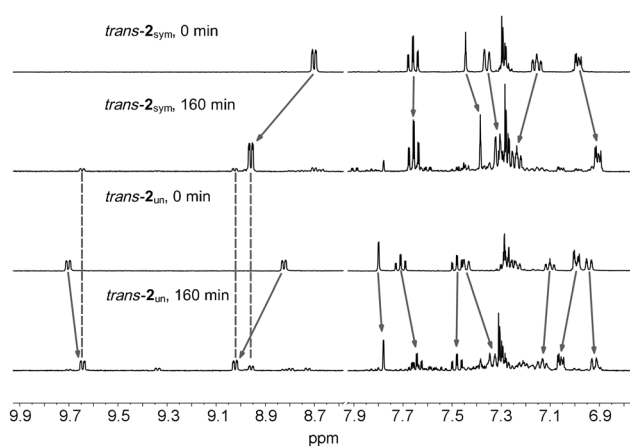
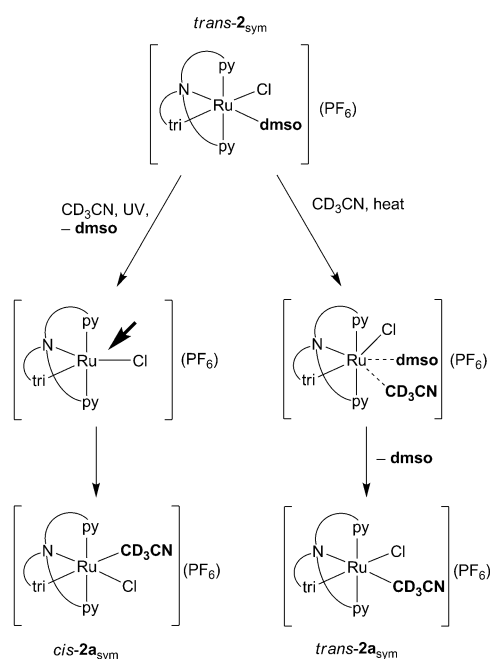


Figure 13. Changes in the ^1H NMR spectra of $\text{trans-2}_{\text{sym}}$ and $\text{trans-2}_{\text{un}}$ in CD_3CN upon irradiation with UV light.

(see the Supporting Information, Figure S37). Corresponding to this intensity loss, signals of a new symmetrical species emerged. This means that 66% of the molecules that lost their non-deuterated ligand (100%) substituted it for a deuterated dmsO ligand *trans* to the N_{amine} atom, hence keeping their conformation. 33% of the molecules substituted non-deuterated for deuterated DMSO and also changed their conformation, thus forming a new species with two identical pyridine arms (see aromatic region in Figure S37 in the Supporting Information). We assume that this species is the isomer with the dmsO ligand in the position *cis* to the N_{amine} atom, that is, *cis-2}_{\text{sym}}. When $\text{trans-2}_{\text{sym}}$ was irradiated in $[\text{D}_6]\text{DMSO}$ for 760 min, the ^1H NMR signal of coordinated dmsO (3.60 ppm) lost 80% of its original intensity, whereas the other signals lost 44% of their intensity (see the Supporting Information, Figure S41). This result means that of the molecules that substituted the dmsO ligand for $[\text{D}_6]\text{dmsO}$ (80%), more than half changed their conformation (44%), thus forming *cis-2}_{\text{sym}}. Hence, in the case of $\text{trans-2}_{\text{sym}}$, heating favors the substitution of the dmsO ligand with a retention of the original complex conformation, whereas irradiation favors substitution with concomitant isomerization to *cis-2}_{\text{sym}}.***

We therefore assume that the product formed from $\text{trans-2}_{\text{sym}}$ in CD_3CN upon heating is the acetonitrile complex, $\text{trans-2a}_{\text{sym}}$ (Scheme 3). Because irradiation with UV light seems to favor the isomerization of $\text{trans-2}_{\text{sym}}$ and trans-1 (see above) in $[\text{D}_6]\text{DMSO}$, we assume that the complexes formed in CD_3CN upon irradiation are *cis-2a}_{\text{sym}} and *cis-2a}_{\text{un}}. Scheme 3 summarizes our explanation of the observed reactivity. The ^1H NMR spectra also show that upon irradiation, some unsymmetrical *cis-2a}_{\text{un}} is formed from symmetrical $\text{trans-2}_{\text{sym}}$ and some symmetrical *cis-2a}_{\text{sym}} is formed from unsymmetrical $\text{trans-2}_{\text{un}}$ (see dashed lines in Figure 13). The irradiation of $\text{trans-2}_{\text{sym}}$ and $\text{trans-2}_{\text{un}}$ in CD_3CN leads to the following: (a) the substitution of the dmsO ligand for acetonitrile; (b) the isomerization of the complexes with respect to the position of the chlorido ligand; (c) a slight scrambling of the complex conformation with respect to the individual positions of the pyridine and triazole arms. Finally, complexes $\text{trans-3}_{\text{un}}$ and trans-4 do not show****



Scheme 4. Proposed mechanisms for the reaction of *trans-2_{sym}* in CD₃CN under heating and irradiation with UV light.

clean reactions to new species neither upon heating nor upon irradiation with UV light for an extended amount of time. They only show a slight decrease in intensity of their ¹H NMR signals (for example, 10% intensity loss for *trans-4* after 10 h of irradiation at 365 nm).

The formation of different products from *trans-2_{sym}* upon heating and irradiation in CD₃CN can be rationalized by assuming different transition states for the two reactions (Scheme 4). We hypothesize that thermal activation should lead to a weakening of the Ru–S bond and the formation of a 7-coordinate transition state, which should favor the retention of the complex conformation. An MLCT transition, like the oxidation to Ru^{III}, should lead to a breaking of the Ru–S bond and to the formation of a 5-coordinate transition state. Such a transition state would favor an attack of the acetonitrile molecule from the less crowded side opposite to the equatorial arm, thus resulting in a change in conformation with respect to the chlorido ligand. It could also give rise to the observed scrambling of the tripod arms.

Conclusion

Summarizing, we have presented an efficient synthetic route for the generation of mixed-donor tripodal ligands containing both pyridyl and triazolyl arms. With these and other ligands, we have synthesized four new complexes of the series [Ru(Lⁿ)(dmsoligand)Cl](PF₆) (1–4), in which the three pyridylmethyl arms of L¹ (TPA) are successively substituted with triazolylmethyl arms (L⁴ = TBTA, three triazole arms). For L², two isomers, with respect to the position of the single triazole arm (equatorial or axial, *trans-2_{sym}* or *trans-2_{unr}*), were separated and structurally characterized. The substitution of triazole for pyridine arms did

not have a pronounced effect on the oxidation potential of the Ru^{II} center. However, the substitution greatly affects the stability of the Ru–S_{dmsoligand} bond. This stability largely depends on π back donation from the Ru center to the S=O moiety, and it is, therefore, intimately linked to the electron density at the metal center.

When the electron density at the metal center is lowered by either electrochemical oxidation to Ru^{III} or through an MLCT transition in the range 300–450 nm, the dmsoligand becomes labile and can dissociate. This results in a rearrangement of the dmsoligand from the S-bound to the O-bound form in CV experiments, behavior that was observed and simulated for *trans-1*. Furthermore, it results in ligand substitution upon irradiation at 365 nm in CD₃CN, a change that could be monitored by ¹H NMR. The electron density at the Ru center and, hence, the stability of the Ru–S bond increases with the number of triazole arms from complex *trans-1* to *trans-4*. This increase is evidenced by the increasing reversibility of the oxidation process in the CV and an increasingly inert behavior under irradiation or heating in coordinating solvents. Interestingly, the stability of the Ru–S bond is not only sensitive to the number of triazole arms but also to their position. Complex *trans-2_{unr}*, which has one triazole arm in an axial position, shows a much more reversible oxidation wave in the CV than its isomer, *trans-2_{sym}* (triazole in the equatorial position). Whereas *trans-2_{unr}* does not react upon heating in CD₃CN, *trans-2_{sym}* forms the acetonitrile complex *trans-2_asym*.

We have thus shown that by the stepwise substitution of triazolylmethyl arms for pyridylmethyl arms, the redox properties and reactivities of metal complexes with tripodal N₄ ligands can be finely tuned. Even though the complex *trans-1* has been known in the literature for a while,^[3,14] this is the first time that redox-induced ligand exchange in that complex has been thoroughly investigated and quantified through simulations of the cyclic voltammograms. In combination with the advantages offered by triazole click chemistry (preparational ease, chemical stability, substituent versatility), this ligand family is a promising platform for catalyst design and tuning, as well as for photocatalysis and redox catalysis. Further research to thoroughly characterize the ligand-exchange products, to broaden the ligand exchange beyond solvent molecules, and to apply the complexes as oxidation catalysts are currently under way in our laboratories.

Experimental Section

General procedures

All chemicals were commercially available and used as purchased unless otherwise noted. Solvents used for synthesis were dried with appropriate drying agents. All manipulations were carried out under a nitrogen atmosphere unless otherwise noted. The precursor [Ru(dmsoligand)₄Cl₂]^[16] complex *trans-1*,^[3] and the ligands TPA^[9] and TBTA,^[10] were synthesized according to literature procedures. The ligands L² [*N*-(1-benzyl-1H-1,2,3-triazol-4-yl)methyl-*N,N*-di(2-pyridylmethyl)amine] and L³ [*N,N*-di(1-benzyl-1H-1,2,3-triazol-4-yl)methyl-*N*-(2-pyridyl)methylamine] were prepared according to modified literature procedures, which are described in the Supporting Infor-

mation. ^1H NMR data were recorded with a Jeol Lambda 400 (400 MHz) by using the chemical shift of the solvent as an internal standard. X-band EPR spectra were recorded at 110 K with an EMX Bruker system connected to an ER 4131 VT (variable-temperature) accessory. The EPR samples were electrolyzed with a platinum-wire working electrode and a platinum-wire counter electrode. Elemental analyses (CHN) were measured with an Elementar Vario EL III and a PerkinElmer Analyzer 240. Mass spectra were recorded with an Agilent 6210 ESI-TOF spectrometer (Agilent Technologies, Santa Clara, CA, USA).

Electrochemistry

Cyclic voltammograms were recorded with a PAR VersaStat 4 potentiostat (Ametek) by working in anhydrous dichloromethane ($\text{H}_2\text{O} \leq 0.005\%$, puriss., Sigma Aldrich) or acetonitrile ($\text{H}_2\text{O} \leq 0.01\%$, puriss., Sigma Aldrich) distilled from calcium hydride or calcium chloride, respectively. A three-electrode setup was used with a glassy-carbon working electrode, a coiled platinum wire as the counter electrode, and a coiled silver wire as the pseudo reference. Ferrocene or decamethylferrocene were used as an internal standard, and 0.1 M NBu_4PF_6 (Fluka, $\geq 99.0\%$, electrochemical grade) was used as an electrolyte. Simulations of the CV data were carried out with the software, DigiElch Professional (Version 7.FD), and details of the simulation are given in the Supporting Information.

UV/Vis spectroscopy and spectroelectrochemistry

UV/Vis spectra were recorded with an Avantes spectrometer consisting of a light source (AvaLight-DH-S-Bal), a UV/Vis detector (AvaSpec-ULS2048), and a NIR detector (AvaSpec-NIR256-TEC). UV/Vis spectroelectrochemistry measurements were carried out in an optically transparent thin-layer electrochemical (OTTLE) cell^[17] with a platinum-mesh working electrode, an platinum-mesh counter electrode, and a silver-foil pseudo reference.

Reactivity experiments

The reactivity experiments of the complexes were carried out in deuterated solvents in NMR tubes sealed with parafilm with complex concentrations of 3 mmol L^{-1} . The NMR tubes were either heated at 80°C in an oil bath or irradiated with a 4 W UV lamp at 365 nm.

X-ray crystallography

Single-crystal X-ray diffraction data were collected with a Stoe X-Area or a Bruker Smart AXS diffractometer. Data were collected at 100(2) K by using graphite-monochromated $\text{Mo K}\alpha$ radiation ($\lambda = 0.71073 \text{ \AA}$). The strategy for the data collection was evaluated by using the CrysAlisPro CCD software. The data were collected by the standard ψ - ω scan techniques and were scaled and reduced by using CrysAlisPro RED software. The structures were solved by direct methods using SHELXS-97 and refined by full-matrix least-squares with SHELXL-97, refining on F^2 .^[18]

The positions of all the atoms were obtained by direct methods. All non-hydrogen atoms were refined anisotropically. The remaining hydrogen atoms were placed in geometrically constrained positions and refined with isotropic temperature factors, generally 1.2 times the U_{eq} values of their parent atoms. Table S2 contains the parameters for the data collection and refinement.

CCDC-918970 (for *trans-2*_{sym}-acetone), 918971 (for *trans-3*_{un}), and 949830 (for *trans-2*_{un}) contain the crystallographic information for this paper. All these data can be obtained free of charge from the

Cambridge Crystallographic Data Centre via www.ccdc.cam.ac.uk/data_requests/cif.

General procedure for the preparation of the complexes

$[\text{Ru}(\text{dmsO})_4\text{Cl}_2]$ (1 equiv), the tripodal ligand, L_n (1 equiv), and KPF_6 (1.5 equiv) were heated at reflux in methanol (20 mL) overnight (ca. 12 h). The work-up was carried out under ambient conditions with commercially available non-dried solvents. After cooling to room temperature, the reaction mixture was concentrated (to ca. 5 mL) by evaporation of the solvent, and Et_2O (ca. 30 mL) was added to precipitate the crude product. The crude product was dried in a vacuum and purified by column chromatography on aluminum oxide (5 wt.-% water) with $\text{CH}_2\text{Cl}_2/\text{methanol}$ (99:1 v/v) as an eluent.

cis-1: L^1 (TPA, 90 mg, 0.31 mmol), $[\text{Ru}(\text{dmsO})_4\text{Cl}_2]$ (145 mg, 0.30 mmol), and KPF_6 (83 mg, 0.45 mmol) were reacted in methanol (20 mL). After work-up and purification by column chromatography, the complex was precipitated from the concentrated eluent by addition of diethyl ether, and it was obtained as a yellow powder (130 mg, 0.195 mmol, 65% yield). ^1H NMR (CD_3CN , 400 MHz): $\delta = 2.82$ (s, 6H; dmsO), 4.46 (s, 2H; $\text{CH}_2(\text{eq})$), 4.64 (ABq, $J_{\text{AB}} = 16 \text{ Hz}$, 2H; $\text{CH}_2(\text{ax})$), 5.37 (ABq, $J_{\text{AB}} = 16 \text{ Hz}$, 2H; $\text{CH}_2(\text{ax})$), 7.09 (d, $J = 8 \text{ Hz}$, 1H; py(eq)), 7.27 (t, $J = 8 \text{ Hz}$, 2H; py(ax)), 7.31 (t, $J = 7 \text{ Hz}$, 1H; py(eq)), 7.40 (d, $J = 8 \text{ Hz}$, 2H; py(ax)), 7.64 (dt, $J_1 = 8 \text{ Hz}$, $J_2 = 1.6 \text{ Hz}$, 1H; py(eq)), 7.74 (dt, $J_1 = 8 \text{ Hz}$, $J_2 = 1.6 \text{ Hz}$, 2H; py(ax)), 8.73 (d, $J = 8 \text{ Hz}$, 2H; py(ax)), 9.67 ppm (d, $J = 8 \text{ Hz}$, 1H, py(eq)); UV/Vis (CH_2Cl_2): λ ($\epsilon/10^4 \text{ m}^{-1} \text{ cm}^{-1}$) = 250 (1.62), 316 (0.70), 366 (1.06), 425 nm (sh; 0.08); HRMS (ESI): m/z calcd for $\text{C}_{18}\text{H}_{18}\text{N}_6\text{RuCl}$, $[\text{Ru}(\text{L}^1)\text{Cl}(\text{N}_2)]^+$: 455.0325 and $\text{C}_{20}\text{H}_{24}\text{N}_4\text{RuClSO}$, $[\text{Ru}(\text{L}^1)\text{Cl}(\text{dmsO})]^+$, 505.0403; found: 455.0341 and 505.0417; elemental analysis calcd (%) for $\text{C}_{20}\text{H}_{24}\text{N}_4\text{RuSOClPF}_6 \cdot 0.25\text{Et}_2\text{O}$: C 37.73, H 4.00, N 8.38; found: C 37.85, H 3.99, N 8.31.

trans-2: L^2 (195 mg, 0.5 mmol), $[\text{Ru}(\text{dmsO})_4\text{Cl}_2]$ (242 mg, 0.5 mmol), and KPF_6 (137 mg, 0.75 mmol) were reacted in methanol (20 mL). After work-up and purification by column chromatography, the complex was precipitated from the concentrated eluent by addition of diethyl ether, and it was obtained as a yellow powder. At this stage, the compound still contained both isomers, *trans-2*_{sym} and *trans-2*_{un}. It was submitted to column chromatography once more, and, this time, the eluent gradient was carefully raised from pure CH_2Cl_2 to $\text{CH}_2\text{Cl}_2/\text{methanol}$ 98:2 v/v. The first of two fractions afforded pure *trans-2*_{un} as a yellow powder after concentration and precipitation by addition of diethyl ether (130 mg, 0.159 mmol, 32% yield). The second fraction contained *trans-2*_{sym} (72 mg, 0.088 mmol, 18% yield). Single crystals of *trans-2*_{sym}-acetone suitable for X-ray diffraction analysis were obtained by condensing diethyl ether onto a concentrated solution of the complex in acetone. Single crystals of *trans-2*_{un} suitable for X-ray diffraction analysis were obtained by condensing diethyl ether onto a concentrated solution of the complex in ethyl acetate. Data for *trans-2*_{sym}: ^1H NMR (CD_3CN , 400 MHz): $\delta = 3.60$ (s, 6H; dmsO), 4.37 (s, 2H; $\text{CH}_2(\text{eq})$), 4.77 (ABq, $J_{\text{AB}} = 15 \text{ Hz}$, 2H; $\text{CH}_2(\text{ax})$), 5.40 (s, 2H; $\text{CH}_2(\text{benzyl}, \text{eq})$), 5.69 (ABq, $J_{\text{AB}} = 15 \text{ Hz}$, 2H; $\text{CH}_2(\text{ax})$), 6.96–7.01 (m, 2H, aryl), 7.15 (t, $J = 8 \text{ Hz}$, 2H; py(ax)), 7.25–7.31 (m, 3H; aryl), 7.36 (d, $J = 8 \text{ Hz}$, 2H; py(ax)), 7.45 (s, 1H; triazole), 7.66 (dt, $J_1 = 8 \text{ Hz}$, $J_2 = 1.6 \text{ Hz}$, 2H, py(ax)), 8.70 ppm (d, $J = 8 \text{ Hz}$, 2H; py(ax)); UV/Vis (CH_2Cl_2): λ ($\epsilon/10^4 \text{ m}^{-1} \text{ cm}^{-1}$) = 255 (1.02), 318 (0.65), 389 (sh; 0.64), 412 nm (0.73); HRMS (ESI): m/z calcd for $\text{C}_{22}\text{H}_{22}\text{N}_8\text{RuCl}$ $[\text{Ru}(\text{L}^2)\text{Cl}(\text{N}_2)]^+$ 535.0699; found 535.0699; elemental analysis calcd (%) for $\text{C}_{24}\text{H}_{28}\text{N}_6\text{RuSOClPF}_6 \cdot \text{CH}_2\text{Cl}_2$ (mixture of both isomers): C 36.84, H 3.71, N 10.31; found: C 37.25, H 3.94, N 10.33. Data for *trans-2*_{un}: ^1H NMR (CD_3CN , 400 MHz): $\delta = 3.35$ (s, 3H; dmsO), 3.49 (s,

3H; dmsO), 4.58 (ABq, $J_{AB} = 14$ Hz, 1H; CH₂), 4.59 (s, 2H; CH₂), 4.79 (ABq, $J_{AB} = 15$ Hz, 1H; CH₂), 5.10 (ABq, $J_{AB} = 14$ Hz, 1H; CH₂), 5.41 (ABq, $J_{AB} = 15$ Hz, 1H; CH₂), 5.47 (ABq, $J_{AB} = 15$ Hz, 1H; CH₂), 5.72 (ABq, $J_{AB} = 15$ Hz, 1H; CH₂), 6.94 (d, $J = 8$ Hz, 1H; py), 6.79–7.01 (m, 2H; aryl), 7.10 (t, $J = 8$ Hz, 1H; py), 7.21–7.33 (m, 4H; aryl and py), 7.44 (d, $J = 8$ Hz, 1H; py), 7.48 (dt, $J_1 = 8$ Hz, $J_2 = 1.6$ Hz, 1H; py), 7.71 (dt, $J_1 = 8$ Hz, $J_2 = 1.6$ Hz, 1H; py), 7.80 (s, 1H; triazole), 8.82 (d, $J = 8$ Hz, 1H; py), 9.70 ppm (d, $J = 8$ Hz, 1H; py); UV/Vis (CH₂Cl₂): λ ($\epsilon/10^4$ m⁻¹ cm⁻¹) = 252 (1.01), 315 (sh; 0.53), 350 (0.74), 380 nm (0.80).

trans-3: L³ (225 mg, 0.5 mmol), [Ru(dmsO)₄Cl₂] (242 mg, 0.5 mmol), and KPF₆ (137 mg, 0.75 mmol) were reacted in methanol (20 mL). After work-up and purification by column chromatography, the complex was precipitated from the concentrated eluent by addition of diethyl ether, and it was obtained as a yellow powder (260 mg, 0.293 mmol, 58% yield). Single crystals of *trans-3*_{un} suitable for X-ray diffraction analysis were obtained by condensing diethyl ether onto a concentrated solution of the complex in ethyl acetate. Data for *trans-3*_{un}: ¹H NMR (CD₃CN, 400 MHz): $\delta = 3.35$ (s, 3H; dmsO), 3.76 (s, 3H; dmsO), 4.22 (ABq, $J_{AB} = 17$ Hz, 1H; CH₂), 4.46 (ABq, $J_{AB} = 18$ Hz, 1H; CH₂), 4.64 (ABq, $J_{AB} = 14$ Hz, 1H; CH₂), 4.75 (ABq, $J_{AB} = 15$ Hz, 1H; CH₂), 5.13 (ABq, $J_{AB} = 14$ Hz, 1H; CH₂), 5.44 (ABq, $J_{AB} = 18$ Hz, 1H; CH₂), 5.46 (s, 2H; CH₂(benzyl)), 5.56 (ABq, $J_{AB} = 14$ Hz, 1H; CH₂), 6.93–6.99 (m, 2H; aryl), 7.14 (t, $J = 8$ Hz, 1H; py), 7.21–7.38 (m, 9H; aryl and py), 7.46 (s, 1H; triazole), 7.61 (dt, $J_1 = 8$ Hz, $J_2 = 1.6$ Hz, 1H; py), 7.83 (s, 1H; triazole), 9.29 ppm (d, $J = 8$ Hz, 1H; py); UV/Vis (CH₂Cl₂): λ ($\epsilon/10^4$ m⁻¹ cm⁻¹) = 254 (0.66), 313 (0.79), 367 (0.73), 391 nm (0.54); HRMS (ESI): *m/z* calcd. for C₂₆H₂₆N₁₀RuCl, [Ru(L³)Cl(N₂)⁺ 615.1055 and C₂₈H₃₂N₈RuClSO, [Ru(L³)Cl(dmsO)]⁺, 665.1131; found: 615.1074 and 665.1152; elemental analysis calcd. (%) for C₂₈H₃₂N₈RuSOCI PF₆·C₂H₆SO: C 40.56, H 4.31, N 12.61; found: C 40.56, H 4.46, N 12.80.

trans-4: L⁴ (TBTA, 205 mg, 0.38 mmol), [Ru(dmsO)₄Cl₂] (184 mg, 0.38 mmol), and KPF₆ (105 mg, 0.57 mmol) were reacted in methanol (20 mL). After work-up and purification by column chromatography, the complex was precipitated from the concentrated eluent by addition of diethyl ether, and it was obtained as a yellow powder (228 mg, 0.150 mmol, 62% yield). ¹H NMR (CD₃CN, 400 MHz): $\delta = 3.44$ (s, 6H; dmsO), 4.27 (s, 2H; CH₂(eq)), 4.61 (ABq, $J_{AB} = 14$ Hz, 2H; CH₂(ax)), 5.10 (ABq, $J_{AB} = 14$ Hz, 2H; CH₂(ax)), 5.34 (s, 2H; CH₂(benzyl,eq)), 5.43 (ABq, $J_{AB} = 15$ Hz, 2H; CH₂(benzyl,ax)), 5.47 (ABq, $J_{AB} = 15$ Hz, 2H; CH₂(benzyl,ax)), 7.13–7.20 (m, 6H; aryl), 7.30–7.37 (m, 9H; aryl), 7.44 (s, 1H; triazole(eq)), 7.77 ppm (s, 2H; triazole(ax)); UV/Vis (CH₂Cl₂): λ ($\epsilon/10^4$ m⁻¹ cm⁻¹) = 255 (0.31), 308 (sh; 0.83), 335 (0.98), 382 nm (sh; 0.13); HRMS (ESI): *m/z* calcd (%) for C₃₂H₃₆N₁₂RuClSO, [Ru(L⁴)Cl(dmsO)]⁺: 745.1526; found: 745.1540; elemental analysis calcd. (%) for C₃₂H₃₆N₈RuSOCI PF₆·C₂H₆SO: C 42.17, H 4.37, N 14.46; found: C 42.83, H 4.44, N 14.62.

Acknowledgement

Felix Führer is acknowledged for experimental work in the synthesis of the complexes.

Keywords: click chemistry · cyclic voltammetry · ligand substitution · ruthenium · tripodal ligands

- [1] For selected examples, see: a) J. Shearer, C. X. Zhang, L. N. Zakharov, A. L. Rheingold, K. D. Karlin, *J. Am. Chem. Soc.* **2005**, *127*, 5469; b) A. Beni, A. Dei, S. Laschi, M. Rizzitano, L. Sorace, *Chem. Eur. J.* **2008**, *14*, 1804; c) Y.-M. Chiou, L. Que, Jr., *J. Am. Chem. Soc.* **1995**, *117*, 3999; d) R.-J. Wei, J. Tao, R.-B. Huang, L.-S. Zheng, *Inorg. Chem.* **2011**, *50*, 8553;

- e) K. S. Min, A. G. DiPasquale, A. L. Rheingold, H. S. White, J. S. Miller, *J. Am. Chem. Soc.* **2009**, *131*, 6229; f) J. Tao, H. Maruyama, O. Sato, *J. Am. Chem. Soc.* **2006**, *128*, 1790; g) K. S. Min, A. G. DiPasquale, J. A. Golen, A. L. Rheingold, J. S. Miller, *J. Am. Chem. Soc.* **2007**, *129*, 2360; h) S. Miyazaki, K. Ohkubo, T. Kojima, S. Fukuzumi, *Angew. Chem.* **2007**, *119*, 923; *Angew. Chem. Int. Ed.* **2007**, *46*, 905; i) Y. Hirai, T. Kojima, Y. Mizutani, Y. Shiota, K. Yoshizawa, S. Fukuzumi, *Angew. Chem.* **2008**, *120*, 5856; *Angew. Chem. Int. Ed.* **2008**, *47*, 5772; j) T. Kojima, T. Morimoto, T. Sakamoto, S. Miyazaki, S. Fukuzumi, *Chem. Eur. J.* **2008**, *14*, 8904; k) F. Weisser, R. Huebner, D. Schweinfurth, B. Sarkar, *Chem. Eur. J.* **2011**, *17*, 5727; l) K. Chen, L. Que, Jr., *Am. Chem. Soc.* **2001**, *123*, 6327; m) K. Chen, M. Costas, J. Kim, A. K. Tipton, L. Que, Jr., *J. Am. Chem. Soc.* **2002**, *124*, 3026; n) J.-H. Ye, L. Duan, C. Yan, W. Zhang, W. He, *Tetrahedron Lett.* **2012**, *53*, 593.
- [2] a) T. Kojima, Y. Hirai, T. Ishizuka, Y. Shiota, K. Yoshizawa, K. Ikemura, T. Ogura, S. Fukuzumi, *Angew. Chem.* **2010**, *122*, 8627; b) M. Yamaguchi, T. Kumano, D. Masui, T. Yamagishi, *Chem. Commun.* **2004**, 798; c) S. Ohzu, T. Ishizuka, Y. Hirai, S. Fukuzumi, T. Kojima, *Chem. Eur. J.* **2013**, *19*, 1563.
- [3] M. Yamaguchi, H. Kousaka, S. Izawa, Y. Ichii, T. Kumano, D. Masui, T. Yamagishi, *Inorg. Chem.* **2006**, *45*, 8342.
- [4] a) V. V. Rostovtsev, L. G. Green, V. V. Fokin, K. B. Sharpless, *Angew. Chem.* **2002**, *114*, 2708; *Angew. Chem. Int. Ed.* **2002**, *41*, 2596; b) C. W. Tornøe, C. Christensen, M. Meldal, *J. Org. Chem.* **2002**, *67*, 3057.
- [5] a) L. Liang, D. Astruc, *Coord. Chem. Rev.* **2011**, *255*, 2933; b) H. Struthers, T. L. Mindt, R. Schibli, *Dalton Trans.* **2010**, *39*, 675; c) J. D. Crowley, D. McMoran in *Topics in Heterocyclic Chemistry*, Vol. 22 (Ed.: J. Kosmrlj), Springer, Berlin/Heidelberg, **2012**, pp. 31; d) D. Schweinfurth, N. Deibel, F. Weisser, B. Sarkar, *Nachr. Chem.* **2011**, *59*, 937.
- [6] For selected examples, see: a) Y. Li, J. C. Huffman, A. H. Flood, *Chem. Commun.* **2007**, 2692; b) D. G. Brown, N. Sanguantrakun, B. Schulz, U. S. Schubert, C. P. Berlinguette, *J. Am. Chem. Soc.* **2012**, *134*, 12354; c) D. Schweinfurth, R. Pattacini, S. Strobel, B. Sarkar, *Dalton Trans.* **2009**, 9291; d) D. Schweinfurth, S. Strobel, B. Sarkar, *Inorg. Chim. Acta* **2011**, *374*, 253; e) D. Schweinfurth, N. Büttner, S. Hohloch, N. Deibel, J. Klein, B. Sarkar, *Organometallics* **2013**, *32*, 5834; f) C. B. Anderson, A. B. S. Elliot, J. E. M. Lewis, C. J. McAdam, K. C. Gordon, J. D. Crowley, *Dalton Trans.* **2012**, *41*, 14625; g) M. Ostermeier, M.-A. Berlin, R. M. Meudtner, S. Demeshko, F. Meyer, C. Limberg, S. Hecht, *Chem. Eur. J.* **2010**, *16*, 10202; h) B. Pinter, D. Urankar, A. Pevec, F. de Proft, J. Kosmrlj, *Inorg. Chem.* **2013**, *52*, 4528; i) D. Schweinfurth, C.-Y. Su, S.-C. Wei, P. Braunstein, B. Sarkar, *Dalton Trans.* **2012**, *41*, 12984; j) M. Mydlak, C. Bizzarri, D. Hartmann, W. Sarfert, G. Schmid, L. De Cola, *Adv. Funct. Mater.* **2010**, *20*, 1812.
- [7] a) H. A. Michaels, C. S. Murphy, R. J. Clark, M. W. Davidson, L. Zhu, *Inorg. Chem.* **2010**, *49*, 4278; b) S. I. Presolski, V. Hong, S.-H. Cho, M. Finn, *J. Am. Chem. Soc.* **2010**, *132*, 14570; c) J. Rosenthal, S. J. Lippard, *J. Am. Chem. Soc.* **2010**, *132*, 5536; d) Y. Zhou, K. Liu, J.-Y. Li, Y. Fang, T.-C. Zhao, C. Yao, *Org. Lett.* **2011**, *13*, 1290; e) S. Huang, R. J. Clark, L. Zhu, *Org. Lett.* **2007**, *9*, 4999; f) C. Orain, N. LePoul, A. Gomila, J.-M. Kerbaol, N. Cosquer, O. Reinaud, F. Conan, Y. LeMest, *Chem. Eur. J.* **2012**, *18*, 594; g) T. J. Simmons, J. R. Allen, D. R. Morris, R. J. Clark, C. W. Levenson, M. W. Davidson, L. Zhu, *Inorg. Chem.* **2013**, *52*, 5838; h) N. Ségaud, J.-N. Rebilly, K. Sénéchal-David, R. Guillot, L. Billon, J.-P. Baltaze, J. Farjon, O. Reinaud, F. Banse, *Inorg. Chem.* **2013**, *52*, 691.
- [8] a) D. Schweinfurth, F. Weisser, D. Bubrin, L. Bogani, B. Sarkar, *Inorg. Chem.* **2011**, *50*, 6114; b) D. Schweinfurth, J. Krzystek, I. Schapiro, S. Demeshko, J. Klein, J. Telsler, A. Ozarowski, C.-Y. Su, F. Meyer, M. Atanasov, F. Neese, B. Sarkar, *Inorg. Chem.* **2013**, *52*, 6880; c) D. Schweinfurth, J. Klein, S. Hohloch, S. Dechert, S. Demeshko, F. Meyer, B. Sarkar, *Dalton Trans.* **2013**, *42*, 6944; d) D. Schweinfurth, S. Demeshko, M. M. Khusniyarov, S. Dechert, V. Gurram, M. R. Buchmeiser, F. Meyer, B. Sarkar, *Inorg. Chem.* **2012**, *51*, 7592.
- [9] A. L. Ward, L. Elbaz, J. B. Kerr, J. Arnold, *Inorg. Chem.* **2012**, *51*, 4694.
- [10] T. R. Chan, R. Hilgraf, K. B. Sharpless, V. V. Fokin, *Org. Lett.* **2004**, *6*, 2853.
- [11] a) S. Hohloch, C.-Y. Su, B. Sarkar, *Eur. J. Inorg. Chem.* **2011**, 3067; b) S. Hohloch, D. Scheiffele, B. Sarkar, *Eur. J. Inorg. Chem.* **2013**, 3956; c) S. Hohloch, B. Sarkar, L. Nauton, F. Cisnetti, A. Gautier, *Tetrahedron Lett.* **2013**, *54*, 1808.
- [12] a) J. Bjernemose, A. Hazell, C. J. McKenzie, M. F. Mahon, L. P. Nielsen, P. R. Raithby, O. Simonsen, H. Toftlund, J. A. Wolny, *Polyhedron* **2003**, *22*, 875;

- b) D. Masui, M. Yamaguchi, T. Yamagishi, *Acta Crystallogr. E Struct. Rep. Online* **2003**, *59*, m308.
- [13] J. Benet-Buchholz, P. Comba, A. Llobet, S. Roeser, P. Vadivelu, S. Wiesner, *Dalton Trans.* **2010**, *39*, 3315.
- [14] T. Kojima, T. Amano, Y. Ishii, M. Ohba, Y. Okaue, Y. Matsuda, *Inorg. Chem.* **1998**, *37*, 4076.
- [15] a) C. E. Welby, C. R. Rice, P. I. P. Elliott, *Angew. Chem.* **2013**, *125*, 11026; *Angew. Chem. Int. Ed.* **2013**, *52*, 10826; b) K. Garg, J. T. Engle, C. J. Ziegler, J. J. Rack, *Chem. Eur. J.* **2013**, *19*, 11686; c) B. Boff, M. Ali, L. Alexandrova, N. Á. Espinosa-Jalapa, R. O. Saavedra-Díaz, R. Le Lagadec, M. Pfeffer, *Organometallics* **2013**, *32*, 5092.
- [16] I. P. Evans, A. Spencer, G. Wilkinson, *J. Chem. Soc. Dalton Trans.* **1973**, 204.
- [17] M. Krejčík, M. Danek, F. Hartl, *J. Electroanal. Chem.* **1991**, *317*, 179.
- [18] G. M. Sheldrick, SHELX-97, Program for Crystal Structure Refinement, Göttingen, Germany, **1997**.

Received: September 15, 2013

Revised: October 30, 2013